



Article

Procedure for Detection of Stator Inter-Turn Short Circuit in AC Machines Measuring the External Magnetic Field [†]

Remus Pusca ^{1,*}, Raphael Romary ¹, Ezzeddine Touti ^{2,3} , Petru Livinti ⁴ , Ilie Nuca ⁵ and Adrian Ceban ¹

¹ Laboratory of Electrotechnical and Environmental Systems, University of Artois, EA 4025 LSEE, F-62400 Béthune, France; raphael.romary@univ-artois.fr (R.R.); apceban@gmail.com (A.C.)

² Department of Electrical Engineering, College of Engineering, University of Northern Border, Arar 1321, Saudi Arabia; touti.these09@gmail.com

³ Department of Electrical Engineering, University of Tunis, Tunis 1008, Tunisia

⁴ Department of Electrical Engineering, Faculty of Engineering, University Vasile Alecsandri of Bacau, 600115 Bacau, Romania; livinti_petru@yahoo.com

⁵ Department of Electrical Engineering, Technical University of Moldova, MD-2004 Chisinau, Moldova; nuca_ilie@yahoo.com

* Correspondence: remus.pusca@univ-artois.fr

[†] This paper is an extended version of our paper published in 2012 XXth International Conference on Electrical Machines, Marseille, France, 2–5 September 2012; pp. 1637–1642.

Abstract: This paper presents a non-invasive procedure to detect inter-turn short circuit faults in the stator windings of AC electrical machines. It proposes the use of the stray external magnetic field measured in the vicinity of the machine to determine stator faults. The originality introduced by this procedure is the analysis method presented in the paper, which when compared to usual diagnosis methods, does not require any data on the healthy state of the machine. The procedure uses the magnetic unbalance created by the rotor poles and the load variation in faulty cases. The presented method can be applied to induction and synchronous machines used as a motor or generator. It is based on the variation of sensitive spectral lines obtained from the external magnetic field when the load changes. Analytical relationships are developed in the paper to justify the proposed method and to explain the physical phenomenon. To illustrate these theoretical considerations, practical experiments are also presented.

Keywords: AC machines; magnetic field; non-invasive fault diagnosis; spectral analysis



Citation: Pusca, R.; Romary, R.; Touti, E.; Livinti, P.; Nuca, I.; Ceban, A. Procedure for Detection of Stator Inter-Turn Short Circuit in AC Machines Measuring the External Magnetic Field. *Energies* **2021**, *14*, 1132. <https://doi.org/10.3390/en14041132>

Academic Editor: Anouar Belahcen

Received: 25 January 2021

Accepted: 17 February 2021

Published: 20 February 2021

Publisher's Note: MDPI stays neutral with regard to jurisdictional claims in published maps and institutional affiliations.



Copyright: © 2021 by the authors. Licensee MDPI, Basel, Switzerland. This article is an open access article distributed under the terms and conditions of the Creative Commons Attribution (CC BY) license (<https://creativecommons.org/licenses/by/4.0/>).

1. Introduction

In recent decades the reliability and the operational safety of electrical machines become an essential issue, so many research studies are focused on their monitoring, which is a crucial phase to prevent severe unexpected failure [1]. For that, the development of acquisition, analysis, and decision techniques are necessary to ensure the detection and diagnosis of electrical machines. The success of these techniques requires a good knowledge of the machine and its behavior in the presence of an internal fault. Among all the diagnosis methods used for rotating electrical machines, one can find:

- methods of appreciation, including techniques that use artificial intelligence [2,3];
- methods for the identification and estimation of physical parameters of the machine [4];
- methods based on modeling of signals that analyze the time variation and the spectral content of different physical quantities. The work presented in this paper concerns that kind of analysis.

For detection of electrical and mechanical faults in electrical AC machines, different techniques have been tested as those based on spectral analysis of the machine's vibrations [5] or current signature analysis [6–10]. However, the interpretation of results requires

an expertise level even more advanced than the method hereto described, making it difficult to ensure real democratization of those techniques. Therefore, monitoring systems are applied only to systems that require high operational safety (for example, in power generation plants). A reliable diagnosis technique which can detect a failure and avoid total damage of motors or generators with a simple and non-invasive monitoring system is of great importance. For this reason, the technology in this field is still in permanent evolution to develop advanced methods [11–16].

In the 1970s, a new technique using the analysis of external magnetic field was developed by Penman [17]. It is a non-invasive technique and easy to implement. The drawback of the latter is the modeling of the magnetic field which depends on the motor housings with an important shielding effect or on the stator yoke. The determination of the external magnetic field requires the modeling of the internal sources and the ferromagnetic influence and the machine conducting materials. The computation of such a problem can be made using finite element software. However, the accurate modeling requires a large computational effort [18,19], especially when 3D modeling is performed. Another approach consists of adapting analytical solutions existing for simple geometries [20] but these methods, based on simplified geometry and under particular hypotheses, can be hardly exploited for electrical machines. In [21], a method based on the definition of attenuation coefficients can be easily combined with an analytical model of the machine.

Fault detection methods using the external magnetic field analysis are based on the property that any fault changes the magnetic field in the near vicinity of the machine. Difficulties for modeling and in the interpretation of this variable lead to exploit only qualitative features of the spectrum, like the appearance of sensitive spectral lines [22]. More usually, studies on the exploitation of the external magnetic field for fault detection are generally limited to model internal consequences of the fault such as: changes in the m.m.f. distribution [23], interaction with the slotting effect [24], magnetic of electrical unbalance [25]. Other researchers prove that the axial field can provide additional information [26–28]. In [29], it is shown that the analysis of the stray flux after supply disconnection can be useful for diagnosis. Advanced exploitation has been developed to provide deeper information: In [30], a sophisticated inverse problem is used for fault detection. In [31], it is shown that the external magnetic field can give information concerning the location of the fault. To improve the diagnostic process, the use of two flux sensors is proposed in [32]. Furthermore, all the diagnosis methods usually require the knowledge of the healthy state of the machine regardless of the physical variable considered. The fault detection is then based on the comparison of the signature for a given state with that of the presumed healthy state by considering an indicator determined from a measurement that is known to be sensitive to a fault. On the other hand, the machine load can be a disturbing factor for diagnosis, because it induces several healthy states. A further difficulty lies in the fact that the healthy state is practically never known until the failure occurs because the user never records the healthy signature beforehand.

This paper proposes a new solution that exploits the information of the external magnetic field measured around the machine. Generally, the load is a disturbing factor for diagnosis methods. However, in the proposed solution, the load variation is used to improve the diagnosis with the advantage that it does not require the knowledge of the machine's healthy state. The detection of a stator fault is based on a comparison between no-load and load operating conditions. Initially, the analytical modeling of the stray flux analysis in the presence of the stator inter-turn short circuit is proposed. Then, the experimental validation for an induction machine (IM) working in a motor and generator case and a wound smooth rotor synchronous generator are presented. The reliability of the method has been tested in a self-excited induction generator (SEIG) which makes it possible to test an unbalanced load case with large frequency slip. The experimental safety measures that have to be taken to ensure the reliable diagnosis are also presented.

2. Analytical Approach for Healthy Machine

The analytical developments concern first a three-phase, p pole pair induction machine with N^s stator slots and N^r rotor bars per pole pair. In this machine with n^s turns per pole pair, the stator coils are series connected and supplied by three-phase balanced sinusoidal voltage with frequency f (angular frequency ω). For the modeling, it is assumed that the air-gap flux density content b is constant during the load variation and that the considered harmonic components are those generated by i_q^s sinusoidal no load currents of I_0^s rms, where q is the phase number. In the proposed model, the ε^s air-gap magnetomotive force (m.m.f) generated by the stator winding is multiplied by the λ per area unit air-gap permeance (which takes into account the slotting effect) to obtain b .

2.1. Air-Gap Permeance

To determine the expression of the air-gap permeance, a specific model is considered as presented by Figure 1. In this model defined in [33], the slot shape is considered rectangular and the field lines crossing the air-gap are radial.

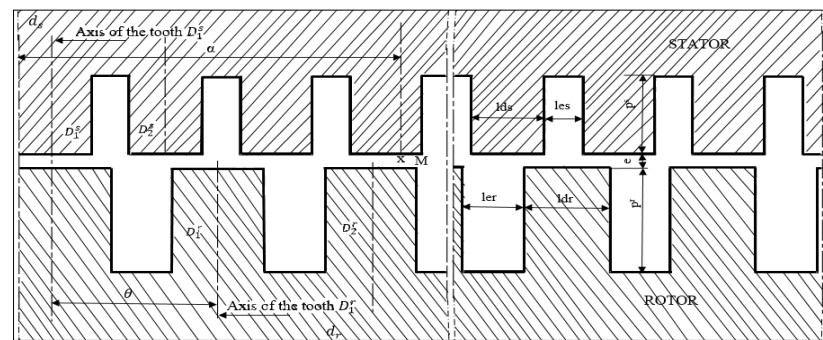


Figure 1. Geometrical parameters of the machine used in the analytical model.

In this model, Λ_{kskr} is a permeance coefficient that depends on the slot geometry:

$$\Lambda_{kskr} = 4\mu_0 A^{sr} \frac{\sin(k_s r_d^s \pi)}{2k_s} \frac{\sin(k_r r_d^r \pi)}{2k_r}, \quad (1)$$

where $\mu_0 = 4\pi 10^{-7}$ is the permeability of the vacuum approximately equal to that of air: $r_d^s = l_d^s / (l_e^s + l_d^s)$, $p^s = l_e^s / 5$, $r_d^r = l_d^r / (l_e^r + l_d^r)$.

In (1) the component, A^{sr} is defined as:

$$A^{sr} = 4p^s p^r \frac{e_M + e}{\pi^2 e^s e^r e_M}, \quad (2)$$

where $e^s = e + p^s$, $e^r = e + p^r$, $e_M = e + p^s + p^r$.

As the field lines never join the bottom of the slots, practically, the air-gap can be modeled considering fictitious slots with a depth equal to the fifth of their opening. With that assumption, λ can be defined as:

$$\lambda = \sum_{ks=-\infty}^{+\infty} \sum_{kr=-\infty}^{+\infty} \Lambda_{kskr} \cos [(ksN^s + krN^r) p \alpha^s - pkrN^r \theta], \quad (3)$$

where θ represents the angular position of the rotor tooth 1 axis relatively to the stator referential d^s tied to the phase 1 axis, ks and kr are negative, null, or positive integers, α^s is the angular abscissa of considered point M in the air-gap related to d^s , and Λ_{kskr} is a permeance coefficient that depends on the slot geometry. Considering the slip s which appears in IM, θ is defined as:

$$\theta = (1 - s)\omega t / p + \theta_0. \quad (4)$$

2.2. Healthy Machine m.m.f

In the healthy machine, the m.m.f ε calculated relatively to the stator d^s can be expressed as:

$$\varepsilon = I_0^s \sum_{h^s} A_{h^s}^s \cos(\omega t - h^s p \alpha^s), \quad (5)$$

where $A_{h^s}^s$ is a function which depends on the winding coefficient corresponding to the rank h^s defined by: $h^s = 6k + 1$, where k varies between $-\infty$ to $+\infty$.

2.3. Air-Gap Flux Density

The calculus developments lead to define $b = \varepsilon^s \lambda$ in the reference frame related to d^s as the following:

$$b = \sum_{h^s, ks, kr} \hat{b}_{h^s k s k r} \cos \left[\begin{array}{c} (1 + krN^r(1 - g))\omega t \\ -p(h^s + ksN^s + krN^r)\alpha^s + krN^r p\theta_0 \end{array} \right], \quad (6)$$

with:

$$\hat{b}_{h^s k s k r} = I_0^s A_{h^s}^s \Lambda_{k s k r}. \quad (7)$$

After regrouping the components of the same frequency and same polarity, it comes:

$$b = \sum_{K, H} b_{K, H}, \quad (8)$$

where $b_{K, H}$ is an elementary component of K frequency rank, and H pole pair number defined as:

$$b_{K, H} = \hat{b}_{K, H} \cos (K\omega t - H\alpha^s - \varphi_{K, H}), \quad (9)$$

and:

$$\left. \begin{array}{l} K = 1 + krN^r(1 - s) \\ H = p(h^s + ksN^s + krN^r) \end{array} \right\}. \quad (10)$$

The frequency rank K only depends on the rotor rank permeance kr . $kr = 0$ leads to define the fundamental ($K = 1$), $kr = \pm 1$ leads to the first slotting harmonics.

2.4. Transverse Field

The stray external magnetic field is obtained from leakage flux created by the different elements of the machine. It is the result of its combination of transverse and axial components. The transverse field measured in the plane perpendicular to the machine axis is an image of the b attenuated by the stator yoke and the axial field located in a plane containing the axis of the machine and created by the overhang effects of the winding. The attenuation caused by the external machine frame will not be taken into account. According to the position of the sensor, the measured field does not come from the same source, and does not result from the same physical phenomenon. Therefore, the measured signal will be sensitive to different field components and it will depend on the position of the sensor around the machine periphery. So, in practice, it is possible to measure mainly the transverse field by choosing an adequate position of the sensor so that the effects of the axial field are minimal. This position corresponds roughly to the middle of the sheet package.

Figure 2 presents a simplified geometry of the machine with the main geometrical parameters which appear in the analytical model with a smooth air gap [34].

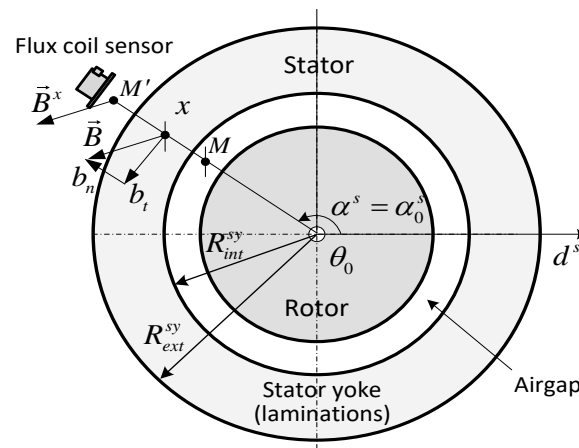


Figure 2. Geometrical parameters of machine used in the analytical model.

In the analytical model used to determine the flux density, only the normal component of the traverse field is considered. It takes into consideration the attenuation coefficient C_H related to the stator yoke that influences the magnitude of $b_{K,H}$ component. It depends on the magnetic permeability μr influenced by the stator lamination, H pole pair number, and the geometrical parameters inner R_{int}^s and outer R_{ext}^s radius and can be defined as follows [35]:

$$C_H = \frac{2}{\mu r \left((R_{int}^s / R_{ext}^s)^{-|H|-1} - (R_{int}^s / R_{ext}^s)^{|H|-1} \right)}. \quad (11)$$

The evolution of C_H versus H pole pair number with $R_{int}^s = 71.6$ mm, $R_{ext}^s = 121$ mm and $\mu r = 1000$ is presented in Figure 3. One can notice that the value of the attenuation coefficient decreases with the increase of H .

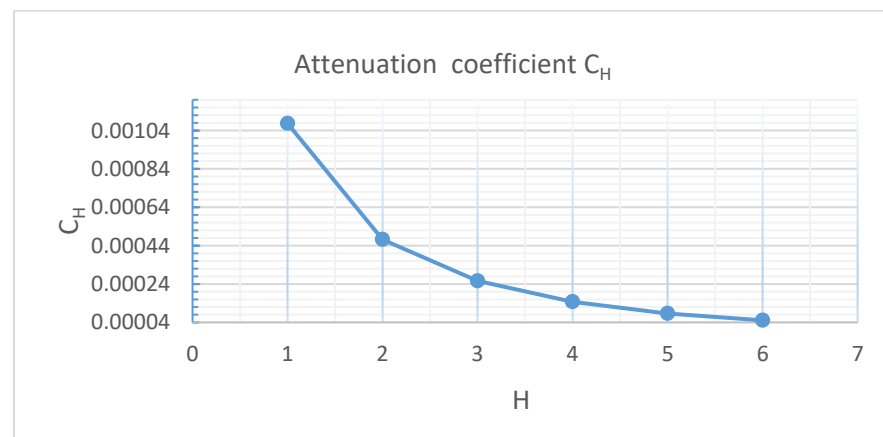


Figure 3. Attenuation coefficient evolution C_H versus pole pair number H .

A physical justification of the evolution given in Figure 3 can be done by considering the line field distribution. Actually, flux density components of high polarity have a line field concentrated at the level of the air-gap whereas those of low polarity have a line field that spreads on the whole stator core. This coefficient influences the amplitude of the traverse flux field.

2.5. Measurement of the Transverse Field

For the proposed diagnosis method, the normal component of the traverse field is measured with flux sensors. The sensors are placed in the closed vicinity of the stator yoke,

allowing to consider in the model only the C_H coefficient. Supposing the sensor placed at radius $x = R_{ext}^s$, the normal traverse flux density b^x is defined as:

$$b^x = \sum_{K,H} C_H \hat{b}_{K,H} \cos (K\omega t - H\alpha^s - \varphi_{K,H}). \quad (12)$$

Let us introduce b_K^x the harmonic of K rank of b^x at the given point M' in the closed vicinity of the stator ($x = R_{ext}^s$, $\alpha^s = \alpha_0^s$), corresponding to the center of the wound flux sensor. b_K^x can be defined by:

$$b_K^x = \hat{b}_K^x \cos (K\omega t - \varphi_K^x). \quad (13)$$

\hat{b}_K^x can be computed by introducing complex quantities:

$$\hat{b}_K^x = \left| \sum_H C_H \hat{b}_{K,H} e^{-j(H\alpha_0^s + \varphi_{K,H})} \right|. \quad (14)$$

At given α_0^s , the resulting flux density harmonics at $K\omega$ angular frequency is composed of several elementary components of different polarity H .

3. Analytical Approach for Faulty Machine

3.1. Structure of the Faulty Machine

In order to determine the influence of the faulty turns in the change of the flux density, a model considering a three-phase stator winding was developed. In this model, it is supposed that “y” turns from the n^s turns of an elementary section belonging to the phase q are short-circuited and that y is small compared with pn^s , the total number of turns per phase. Therefore, it can be assumed that the current remains unchanged and has the same values in each phase in the faulty case. This hypothesis can therefore characterize the short circuit thanks to a model that preserves the original structure of the machine. This model assumes that the stator winding in presence of the fault is equivalent to the healthy winding, associated to “y” independent turns in which the short-circuit current circulates. It will be assumed that these two circuits have independent running. The healthy part of the winding generates therefore the same flux density components without fault.

The model of a faulty winding is presented in Figure 4 where the whole phase winding is composed of an elementary healthy section and one with short circuit turns. For both structures, it is assumed that the magnetic reaction of the rotor is such that only the fundamental of the stator currents for a running at no load will be considered to characterize the air-gap flux density. This way, the resulting air-gap flux density b^* is equal to the initial one, b , to which the flux density b_{sc} generated by the “y” turns flowing through by the current i_{qsc}^s : $b^* = b + b_{sc}$ is added.

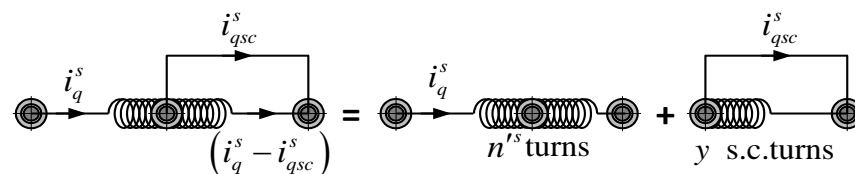


Figure 4. Proposed model for a faulty winding.

The short circuit current is defined as follows:

$$i_{qsc}^s = I_{sc}^s \sqrt{2} \cos(\omega t - \varphi_{sc}). \quad (15)$$

φ_{sc} is the phase lag between the short circuit current and the phase 1 current as shown in Figure 5. This phase actually depends on several parameters such as the impedance

that limits the short circuit current, the short circuit winding, and the position of the fundamental air-gap flux density relative to the phase q current (depending on the load).

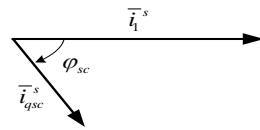


Figure 5. Current diagram in faulty case.

3.2. Faulty Turns m.m.f

The magnetomotive force ε_{qsc}^s generated by the “y” short circuit turns, shifted of α_q^s from ds, is shown on Figure 6 in the case of a 4 poles machine. It also shows the m.m.f ε_{qel}^s generated by the healthy elementary winding. ε_{qsc}^s is an unidirectional m.m.f and can be decomposed in rotating fields that rotate in opposite directions. In a stator referential, ε_{qsc}^s can be written as follows:

$$\varepsilon_{qsc}^s = I_{sc}^s \sum_h A_h^s \cos(\omega t - h\alpha^s - \varphi_h). \quad (16)$$

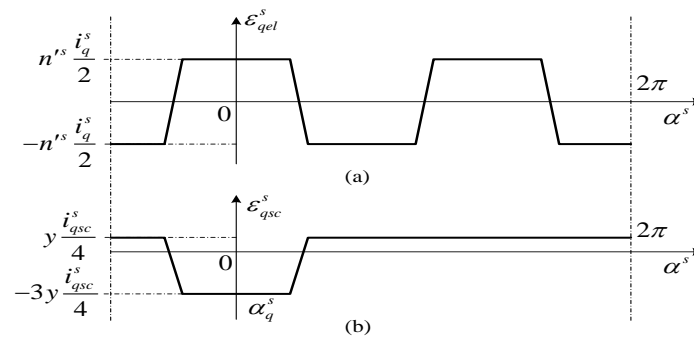


Figure 6. m.m.f generated by the faulty turns.

A_h^s is a function that can be determined from the Fourier series of ε_{qsc}^s and h is a non-null relative integer, which can take consequently all the values of h^s . Here, ϕ_h is defined as: $\phi_h = h\alpha_q^s + \phi_{sc}$.

As $b_{sc} = \lambda \varepsilon_{qsc}^s$, the calculus developments lead to define this quantity in the reference frame related to d^s . A grouping of parameters with same polarity and same frequency provides:

$$\varepsilon_{qsc}^s = I_{sc}^s \sum_h A_h^s \cos(\omega t - h\alpha^s - \varphi_h), \quad (17)$$

$$b_{sc} = \sum_{K_{sc}, H_{sc}} \hat{b}_{sc, K_{sc}, H_{sc}} \cos(K_{sc}\omega t - H_{sc}\alpha^s - \varphi_{sc, K_{sc}, H_{sc}}), \quad (18)$$

with:

$$\left. \begin{aligned} K_{sc} &= 1 + kr'N^r(1-s) \\ H_{sc} &= h + p(k s'N^s + kr'N^r) \end{aligned} \right\}. \quad (19)$$

where ks' and kr' are the permeance rank of the rotor and stator which vary from $-\infty$ to $+\infty$, equivalent to ks and kr defined in (10). $\hat{b}_{sc, K_{sc}}^x$ calculated at the point M' is the harmonic of K rank, of magnitude $\hat{b}_{sc, K_{sc}}^x$:

$$\bar{b}_{sc, K_{sc}}^x = \hat{b}_{sc, K_{sc}}^x \cos(K_{sc}\omega t - \varphi_{sc, K_{sc}}^x), \quad (20)$$

and

$$\hat{b}_{sc, K_{sc}}^x = \left| \sum_H C_H \hat{b}_{sc, K_{sc}, H_{sc}} e^{-j(H\alpha_0^s + \varphi_{sc, K_{sc}, H_{sc}})} \right|. \quad (21)$$

By comparing the values of the frequency rank K_{sc} given by (18), which appears in the case of short circuit with frequency value taken by K in healthy case defined by (10), we can notice that, there is no bring new frequency in the signal spectrum. Therefore, to detect the failure, the classic diagnosis method which analyzes the increase (or decrease) of already existing lines needs to know the amplitude value in the healthy case as a reference, thus limiting their practice application. Concerning the polarities H and H_{sc} , one can observe that H_{sc} can take all positive and negative integers whereas H is a multiple of p . H_{sc} can especially be equal to ± 1 corresponding to components that are weakly attenuated by the stator iron. In the following, the properties relating to the dissymmetry generated by such components will be exploited.

3.3. Searching for Sensitive Components

The harmonic at $K\omega$ angular frequency is composed of several components of various polarities. The ones that have the highest contribution can be found by searching the lowest values of h^s , h , ks , kr , $k's$, $k'r$, leading to the smallest possible H (or H_{sc}) corresponding to the less attenuated components.

Let us consider an induction machine with $p = 2$, $N^s = 24$, $N^r = 16$, supplied by 50 Hz power source. Tables 1 and 2 give the magnitude of the components relative to the magnitude of the fundamental for the healthy and faulty machines respectively. The short circuit current rms value is three times that of the line current: $I_{sc}^s = 3I_0^s$.

Table 1. Components generated by the healthy induction machine.

kr	ks	h^s	K	H	$f(\text{Hz})$	$K \times f(\text{Hz})$	C_H	$\hat{b}_{K,H}^x / \hat{b}_{11}^x$
−1	1	−5	−15	6	50	−750	5.08×10^{-5}	1.48×10^{-5}
−1	1	−11	−15	−6	50	−750	5.08×10^{-5}	4.04×10^{-6}
1	−1	7	17	−2	50	850	4.71×10^{-4}	1.41×10^{-4}
1	−1	13	17	10	50	850	2.66×10^{-6}	2.81×10^{-7}
−2	1	7	−31	−2	50	−1550	4.7×10^{-4}	$−1.28 \times 10^{-4}$
−2	2	−17	−31	−2	50	−1550	4.71×10^{-4}	2.82×10^{-5}

Table 2. Components generated by the faulty induction machine.

$k'r$	$k's$	h^s	K_{SC}	H_{sc}	$K_{sc} \times f(\text{Hz})$	C_H	$\hat{b}_{K_{sc},H_{sc}}^x / \hat{b}_{11}^x$
−1	1	−10	−15	6	−750	5.08×10^{-5}	9.2×10^{-6}
−1	1	−13	−15	3	−750	2.56×10^{-4}	$−3.52 \times 10^{-5}$
−1	1	−14	−15	2	−750	4.71×10^{-4}	$−1.02 \times 10^{-4}$
−1	1	−15	−15	1	−750	0.00107	$−1.84 \times 10^{-4}$
−1	1	−18	−15	−2	−750	4.71×10^{-4}	9.1×10^{-5}
−1	1	−19	−15	−3	−750	2.56×10^{-4}	2.61×10^{-5}
−1	1	−21	−15	−5	−750	8.62×10^{-5}	$−5.8 \times 10^{-6}$
−1	1	−22	−15	−6	−750	5.08×10^{-5}	$−4.07 \times 10^{-6}$
1	−1	10	17	−6	850	5.08×10^{-5}	9.32×10^{-6}
1	−1	11	17	−5	850	8.62×10^{-5}	1.12×10^{-5}
1	−1	14	17	−2	850	4.71×10^{-4}	$−1.02 \times 10^{-4}$
1	−1	15	17	−1	850	0.00107	$−1.9 \times 10^{-4}$
1	−1	17	17	1	850	0.00107	1.82×10^{-4}
1	−1	18	17	2	850	4.71×10^{-4}	9.1×10^{-5}
1	−1	21	17	5	850	8.62×10^{-5}	$−5.8 \times 10^{-6}$
1	−1	22	17	6	850	5.08×10^{-5}	$−4.07 \times 10^{-6}$
−2	1	17	−31	1	−1550	0.00107	$−1.52 \times 10^{-4}$
−2	1	21	−31	5	−1550	8.62×10^{-5}	5.04×10^{-6}
−2	1	22	−31	6	−1550	5.08×10^{-5}	3.26×10^{-6}
−2	2	−26	−31	6	−1550	5.08×10^{-5}	1.92×10^{-6}

In Tables 1 and 2, it can be observed that the highest components in the external magnetic field are mainly issued from air-gap components of the lowest polarity. In healthy conditions, the first slotting harmonics are obtained for:

$Kr = 1, ks = -1, h^s = 7$ lead to $K = 17, H = -2$ ($f = 850$ Hz); $kr = -2, ks = 1, h^s = 7$ lead to $K = -31, H = -2$ ($f = -1550$ Hz); and $kr = -1, ks = 1, h^s = -5$ lead to $K = -15, H = 6$ ($f = -750$ Hz).

In faulty conditions, the same harmonics are obtained for:

$kr' = 1, ks' = -1, h = 15$ lead to $K_{sc} = 17, H_{sc} = -1$ ($f = 850$ Hz); $kr' = -1, ks' = 1, h = -15$ lead to $K_{sc} = -15, H_{sc} = 1$ ($f = -750$ Hz),

and $kr' = -2, ks' = 1, h = 17$ lead to $K_{sc} = -31, H_{sc} = 1$ ($f = -1550$ Hz) with frequencies given for $s = 0$.

In the following, one will consider the harmonics of rank $K = K_{sc} = 17$ ($f = 850$ Hz) because it is generated by components of the lowest polarity in healthy and faulty conditions ($H = -2, H_{sc} = -1$). These components are highlighted in grey in Tables 1 and 2 and they will be considered as the sensitive components for the inter-turn short circuit fault. The sensitivity has been shown in previous works [24]. It can also be noticed that for the healthy machine, only one predominant component can be associated to one given harmonic whereas for the faulty machine, one given harmonic is generated by several components of different polarity and of similar magnitude. In this case, the components with the highest magnitudes has the polarity $H_{sc} = +1$ and $H_{sc} = -1$. Moreover, these components, weakly attenuated by the stator frame, have a magnitude similar to that of the component related to the healthy machine as those highlighted in yellow in Table 2. Therefore, the fault does lead to a significant change in the magnitude of the spectral line at 850 Hz in the external magnetic field. In order to improve the detection, the analysis will be focused on the load-induced variation of sensitive spectral lines measured at two points in the transverse external magnetic field.

3.4. Influence of the Load

Only the sensitive components defined in the previous section are now considered: b_K^x relative to the healthy machine and $b_{sc,K_{sc}}^x$ relative to the faulty machine. They both merge together to generate the resulting harmonic flux density b_K^{*x} . According to the hypothesis related to the rotor magnetic reaction, it will be assumed that \hat{b}_K^x does not change when the load increases. The same hypothesis will be considered for $\hat{b}_{sc,K_{sc}}^x$. Actually, only the phase lag φ_{sc} and consequently ϕ_h change with the load. Consequently, for position 1 (Pos.1) defined for $\alpha^s = 0$, and position 2 (Pos. 2) defined for $\alpha^s = \pi$, the resulting harmonic b_K^{*x} can be expressed as follows:

$$\text{Pos. 1 : } b_K^{*x1} = \hat{b}_K^x \cos(K\omega t - \varphi_K^x) + \hat{b}_{sc,K_{sc}}^x \cos(K_{sc}\omega t - \varphi_{sc,K_{sc}}^x), \quad (22)$$

$$\text{Pos. 2 : } b_K^{*x2} = \hat{b}_K^x \cos(K\omega t - \varphi_K^x) - \hat{b}_{sc,K_{sc}}^x \cos(K_{sc}\omega t - \varphi_{sc,K_{sc}}^x). \quad (23)$$

Considering resulting harmonics, b_K^{*x} obtained from (22) and (23), their difference consists in the sign of the second term $b_{sc,K_{sc}}^x$ which changes in the faulty case as a consequence of the polarity $H_{sc} = 1$ in the expression of cosines ($\cos(\gamma + \pi) = -\cos(\gamma)$), contrary to polarity $H = 2$ of the healthy term when it does not change ($\cos(\gamma + 2\pi) = \cos(\gamma)$). This dissymmetry, generated by the fault in (22) and (23) is, from a physical point of view, the base of the proposed detection procedure. Figure 7a gives the associated time phasor diagram for $\varphi_K^x = 0$. It clearly shows that the magnitudes of the complex quantities \bar{b}_K^{*x1} and \bar{b}_K^{*x2} are different. If the load changes, then a variation of φ_{cc} leads to a variation of $\varphi_{sc,K_{sc}}^x$. Figure 7b gives the time phasor diagram after a variation of $\varphi_{sc,K_{sc}}^x$. It can be observed that the resulting magnitude has increased in Pos. 1 (\hat{b}_K^{*x1}) and has decreased in Pos. 2 (\hat{b}_K^{*x2}). The theoretical approach neglects the phase variation, which leads to a partial justification of the physical phenomenon.

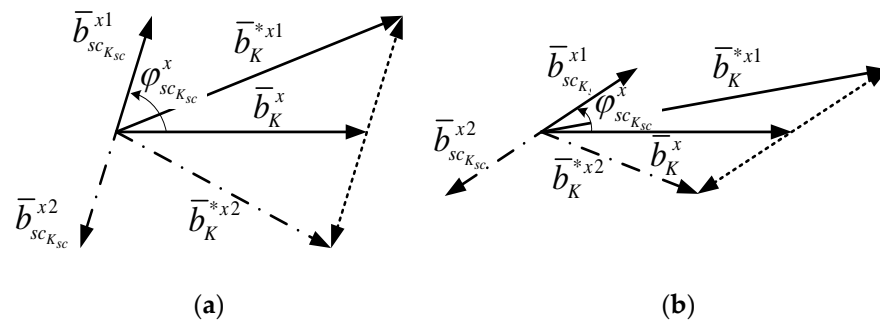


Figure 7. Phasor diagram variation (a) no loaded condition (b) loaded condition.

The different directions of variation between the magnitudes of the \hat{b}_K^{*x} in faulty case allow one to propose the presented procedure:

- In the healthy case:

The air-gap flux density does not change when the machine is loaded compared to the no load case and the term b_{sc,K_sc}^x is null. In this case, the amplitudes of the terms \hat{b}_K^{*x1} and \hat{b}_K^{*x2} measured in Pos. 1 and Pos. 2 keep similar values or at least evolve in the same way if the load of the machine change.

- In the faulty case:

In loaded conditions, the magnitude of the component at $K\omega$ angular frequency measured in Pos. 1 and Pos. 2 will evolve in opposed directions and this particularity is proposed to be exploited in the analysis of the harmonic $K\omega$ as a fault indicator. Compared to another existing proposed methods, one does not require the knowledge of the healthy state to be applied.

3.5. Application to a Salient Pole Synchronous Machine

Different kinds of synchronous machines exist, they differ only by the structure of their rotor: wound salient, or wound smooth rotor (turbo alternator), surface mounted, or interior permanent magnet rotor. The modeling of the intact synchronous machine and the faulty one is deduced from the studied induction machine where the slotting effect created by the dampers is neglected. Since the stator has the same structure for both machines, in the analytical model, it is considered that the effect created by the saliency rotor and wound smooth rotor of the synchronous machine is similar to the rotor slots of the induction machine. Consequently, if the rotor is a wound smooth rotor, the components generated by a healthy and faulty synchronous machine are given by (10) and (18) with particularity $s = 0$. For a salient rotor, as the pole number is equal to the rotor saliencies of the machine, the frequency ranks and pole pair numbers given by (10) can be likewise considered in the case of a synchronous machine, with $N^r = 2$ and $s = 0$:

$$\left. \begin{aligned} K &= 1 + 2kr \\ H &= p(h^s + ksN^s + 2kr) \end{aligned} \right\}. \quad (24)$$

For a faulty machine, (18) becomes:

$$\left. \begin{aligned} K_{sc} &= 1 + 2kr' \\ H_{sc} &= h + p(ks'N^s + 2kr') \end{aligned} \right\}. \quad (25)$$

Tables 3 and 4 give the magnitude of the components relative to the magnitude of the fundamental respectively for the healthy and for the faulty synchronous machines with 4 poles, and $N^s = 18$. The short circuit current rms value is three-time that of the line current: $I_s^{sc} = 3I_0^s$.

Table 3. Components generated by the healthy synchronous machine.

kr	ks	h^s	K	H	$K \times f \text{ (Hz)}$	C_H	$\hat{b}_{K,H}^x / \hat{b}_{11}^x$
6	0	−5	13	14	650	7.2×10^{-6}	6.04×10^{-3}
6	0	1	13	26	650	8.19×10^{-8}	3.43×10^{-3}
7	0	−5	15	18	750	1.63×10^{-6}	13.5×10^{-3}
7	0	1	15	30	750	1.83×10^{-8}	10.8×10^{-3}
−7	0	−5	−13	−38	−650	9.19×10^{-10}	2.21×10^{-3}
−7	0	1	−13	−26	−650	8.19×10^{-8}	2.29×10^{-3}
8	0	−5	17	22	850	3.65×10^{-7}	11.8×10^{-3}
8	0	1	17	34	850	4.01×10^{-9}	8.8×10^{-3}
−8	0	−5	−15	−42	−750	2.05×10^{-10}	4.91×10^{-3}
−8	0	1	−15	−30	−750	1.83×10^{-8}	10.3×10^{-3}

Table 4. Components generated by the faulty synchronous machine.

kr	ks	h^s	K	H	$K \times f \text{ (Hz)}$	C_H	$\hat{b}_{K,H}^x / \hat{b}_{11}^x$
6	0	−5	13	19	650	1.12×10^{-6}	5.13×10^{-4}
6	0	1	13	25	650	1.19×10^{-7}	3.64×10^{-4}
7	0	−5	15	23	750	2.51×10^{-7}	2.13×10^{-3}
7	0	1	15	29	750	2.66×10^{-8}	1.82×10^{-3}
−7	0	−5	−13	−33	−650	5.90×10^{-9}	7.9×10^{-4}
−7	0	1	−13	−27	−650	5.60×10^{-8}	9.8×10^{-4}
8	0	−5	17	27	850	5.60×10^{-8}	1.2×10^{-3}
8	0	1	17	33	850	5.90×10^{-9}	4.8×10^{-4}
−8	0	−5	−15	−37	−750	1.33×10^{-9}	1.46×10^{-4}
−8	0	1	−15	−31	−750	1.26×10^{-8}	1.52×10^{-4}

The results are similar to those of induction machine. It appears that each harmonic at given kr mainly originates from the components of lowest polarity. It also appears that the sensitive harmonics are:

$kr = 7, ks = 0, h^s = -5$ lead to $K = 15, H = 18$ ($f = 750$ Hz); $kr = 7, ks = 0, h^s = 1$ lead to $K = 15, H = 30$ ($f = 750$ Hz);

and $kr = 8, ks = 0, h^s = -5$ lead to $K = 17, H = 22$ ($f = 850$ Hz). In faulty conditions, the same harmonics are obtained for:

$kr = 7, ks = 0, h^s = -5$ lead to $K = 15, H = 23$ ($f = 750$ Hz); $kr = 7, ks = 0, h^s = 1$ lead to $K = 15, H = 29$ ($f = 750$ Hz),

and $kr = 8, ks = 0, h^s = -5$ lead to $K = 17, H = 27$ ($f = 850$ Hz).

In the proposed method, which is the same as in the induction machine, the harmonics obtained for $kr' = \pm 7$ and ± 8 can be analyzed. The choice between two harmonics must be made taking into account as practical measurements of harmonics amplitudes

4. Experimental Results

4.1. Presentation of the IM Test Bench

The tests are performed using a three-phase squirrel-cage induction machine with 4 poles, 50 Hz, 11 kW, 380/660 V, 22.3/13A, 1450 rpm, 48 stator slots, and 32 rotor bars ($N^s = 24, N^r = 16$). This machine presented in Figure 8a is supplied by the grid and is specially modified to enable inter-turn short circuits. For measurement of the external magnetic field, the sensors are 180° spatially shifted around the frame of the machine (Figure 8b). The output connections to the terminal box can short-circuit an elementary section housed in a slot, which corresponds to 12.5% of the full phase winding for the induction machine (Figure 8c).

The equipment above the machine makes it possible to simulate a fault by short-circuiting the coils. The machine can operate under no-load or various loading conditions. For the induction machine, the short circuit current is limited to 15.3 A using an external

rheostat. Figure 8b displays locations 1 and 2 of the flux sensors required for the method. The tests consist of measuring and analyzing the magnetic field outside the machine in order to validate the proposed diagnosis method. The measurements are performed using two identical manufactures wound flux sensors, placed against the machine. It has been checked that the wire current from the machine to the terminal block does not disturb the measurement. As announced in the previous section, the position of sensors must be on the one hand $\alpha_1^s = 0$ (Pos. 1) and, on the other hand, as accurately as possible in $\alpha_2^s = \pi$ with the input (Pos. 2) so that the measurements could be interpreted in the context of the proposed method. For both measurements, the sensor signal measured by the PULSE in the input Signal 1 and Signal 2 is placed in the middle of the machine to reduce the influence of end windings. Tests have been performed on the two induction machines for three operating conditions (motor, generator connected to the power system, and self-excited induction generator).

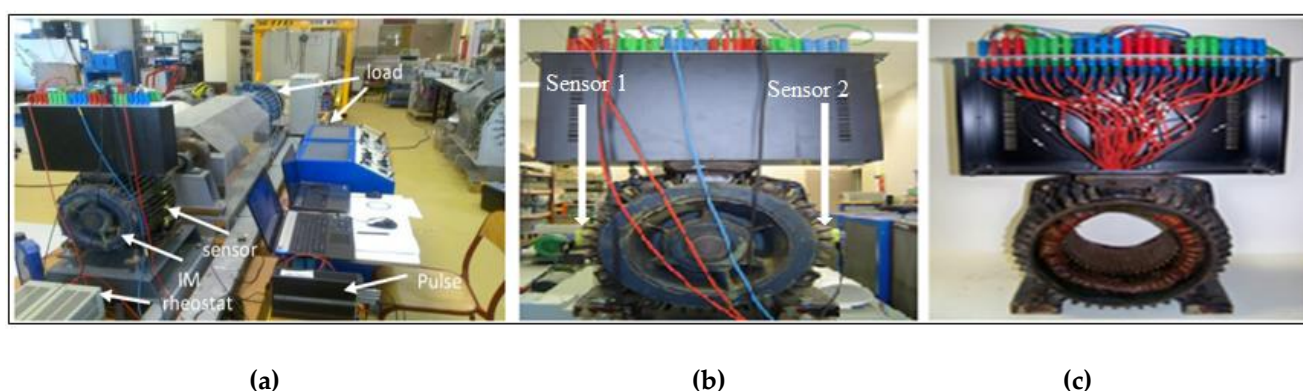


Figure 8. Experimental test bench with special induction machine modified to enable inter-turn short circuits (a) test bench, (b) flux sensors spatially shifted at 180° , (c) stator with a short circuit box and output connections.

4.2. Induction Machine in Motor Case

The time variation of the electromotive force (emf) and the spectrum of the signal delivered by the sensor in the case of the healthy induction machine, measured in the near vicinity of the machine are shown in Figure 9a where the magnitudes are presented in dB. The first tooth harmonics at 750 and 850 Hz can be clearly observed in Figure 9b. The study is focused on the line at 850 Hz, where the theoretical analysis shows a polarity lower than that of the line at 750 Hz. This is reflected by a greater magnitude of the line at 850 Hz, a property that is measured experimentally.

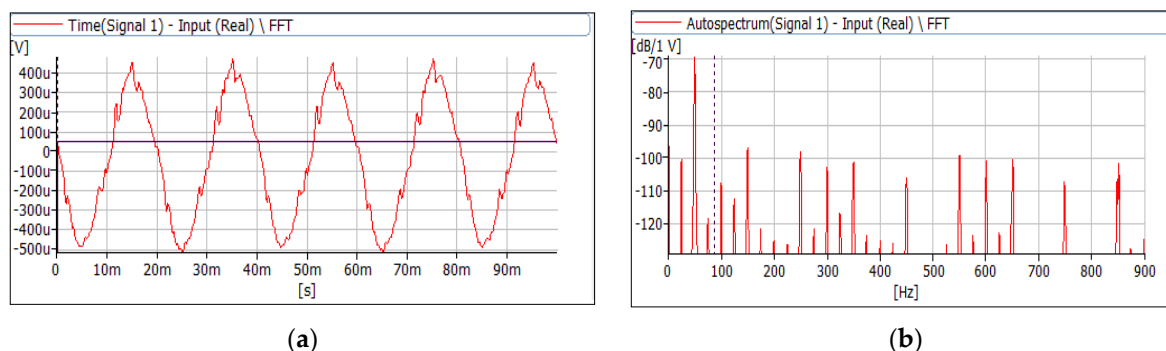


Figure 9. Signal delivered by PULSE acquisition system; (a) emf delivered by flux coil sensor, (b) signal spectrum delivered for the healthy machine.

It should be kept in mind that in practice, the line studied can move with the slip, but will be identified as the line at 850 Hz. The results obtained for this machine operating

as a motor in healthy and short-circuit fault conditions are presented, taking into account the variation of the spectral line at 850 Hz under the load influence. Figure 10a gives the variation of the spectral line at 850 Hz on the signal delivered by the sensor in Pos. 1 and Figure 10b by the sensors in Pos. 2.

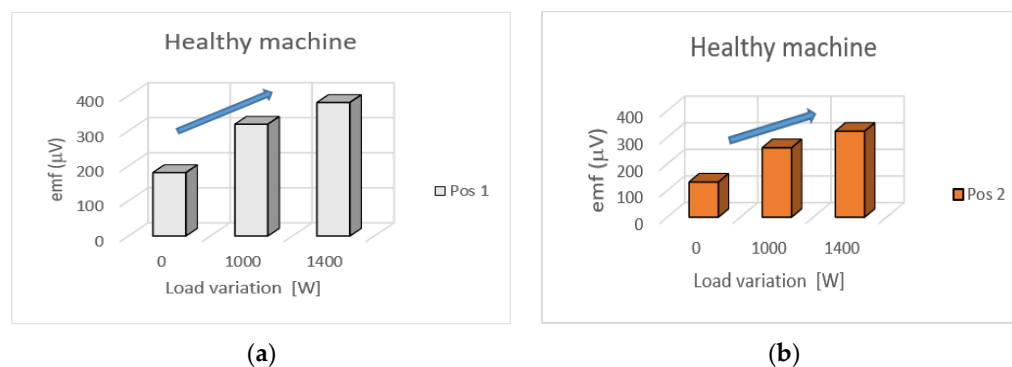


Figure 10. Harmonic components at 850 Hz under both measurement positions for healthy motor and load variation (a) measurement in position 1, (b) measurement in position 2.

Figure 10 shows that a difference appears between the amplitudes of significant lines at 850 Hz for the healthy machine in positions 1 and 2. Actually, due to the real geometry of the machine, the elements that lead to the attenuation are not exactly the same all around the machine. However, as aforementioned in the analytical development, one finds the same direction of variation (positive) of this component for both positions when the machine is loaded.

For the faulty machine (Figure 11), the presence of the shorted turns introduces two-pole flux density components that will be combined with those presented for the healthy machine. Analyzing the results presented above, it can be seen that:

- in healthy conditions, the lines at 850 Hz evolve in the same direction with the change of the load,
- in faulty conditions, the lines at 850 Hz in position 1, compared with those in position 2 vary in opposite directions.
- the value of the short circuit current I_{sc} can influence the evolution of the lines

4.3. Induction Machine in Generator Case

A second test of the proposed method is carried out in the case where the machine is used as a generator connected to the grid. The results are shown in Figure 11.

For this kind of operation, the angle φ_{sc} of short-circuit undergoes a phase change of approximately π compared to motor operating mode. As in the case of motor operation, the obtained results show that for a healthy machine, the magnitudes of lines at 850 Hz increase with the load (Figure 12a). In both measurement positions, they vary in the same direction. For the faulty machine with the short-circuit current I_{sc} limited to 8.2A (Figure 12b) harmonics magnitudes change the variation, its decrease in position 1 for 3.3 kW power load and increase in position 2. Figure 12c,d gives a zoom in the evolution of flux harmonics at frequency 850 Hz measured in Pos. 1 and Pos. 2. The experimental results confirm that the proposed method can be applied also as an induction machine operating as a generator.

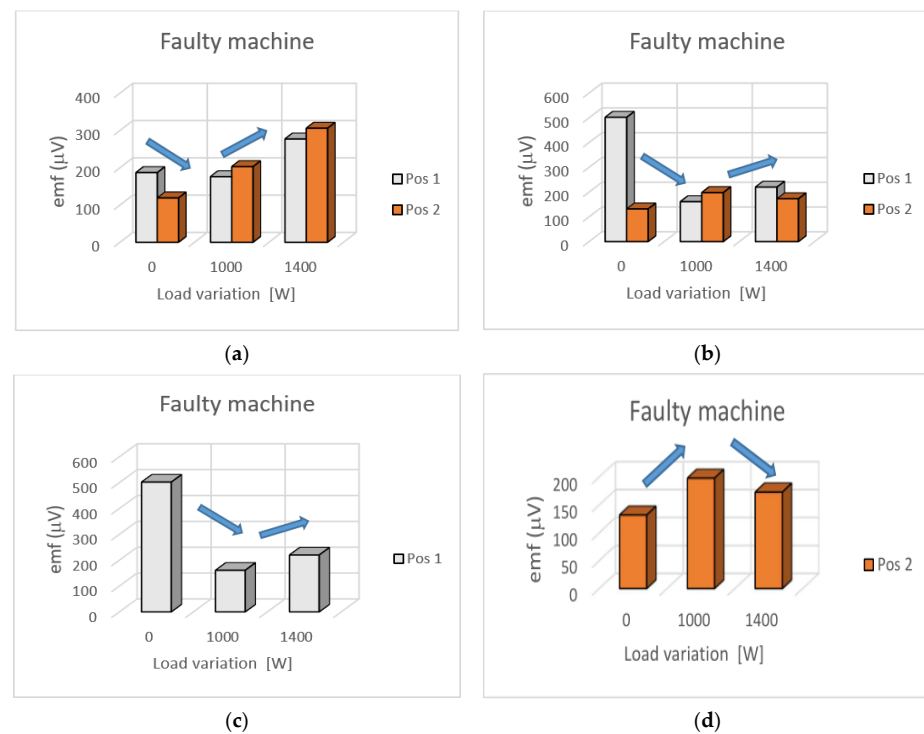


Figure 11. Harmonic components at 850 Hz under both measurement positions for faulty motor and load variation (a) short-circuit current I_{sc} limited at 8.2 A, (b) short-circuit current limited at 15.3 A, (c) load variation for a sensor in position 1 and $I_{sc} = 15.3$ A, (d) load variation for a sensor in position 2 and $I_{sc} = 15.3$ A.

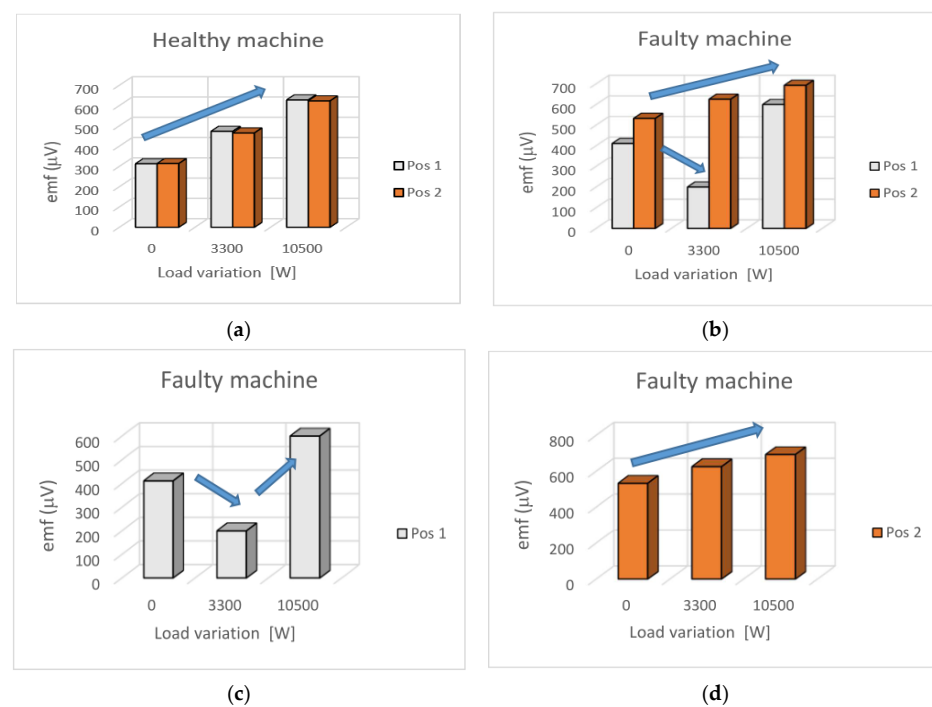


Figure 12. Harmonic components at 850 Hz under both measurement positions for generator operating at load variation in healthy and faulty case: (a) healthy case, (b) faulty case, (c) variation in faulty case for measurement in position 1, (d) variation in the faulty case for measurement in position 2.

4.4. Synchronous Machine

In order to test the efficiency of the proposed method, the following tests are performed on a synchronous machine operating as a generator. This machine is a 4 poles wound smooth rotor (cylindrical rotor) with concentric rotor windings presented in Figure 13 and the following characteristics: 10 kVA, 230/400 V, 25/15 A, 50 Hz, 54 stator slots, ($N^s = 27$), $N^r = 16$, $R_{int}^s = 113.5$ mm, $R_{ext}^s = 165$ mm.

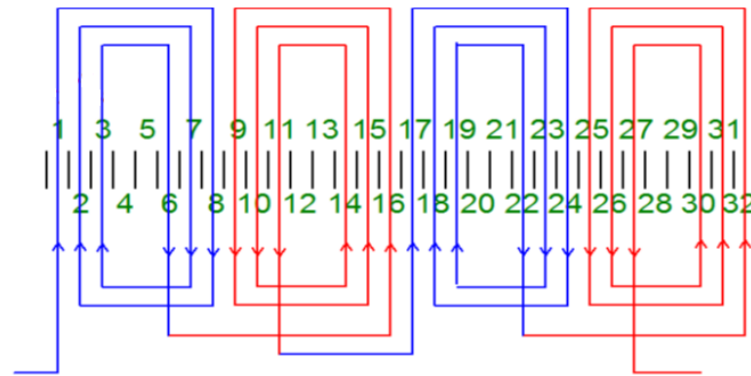


Figure 13. Concentric rotor winding.

A picture of the test bench is shown in Figure 14 where a DC machine is used as a prime mover and external flux sensors are placed around the synchronous generator frame.

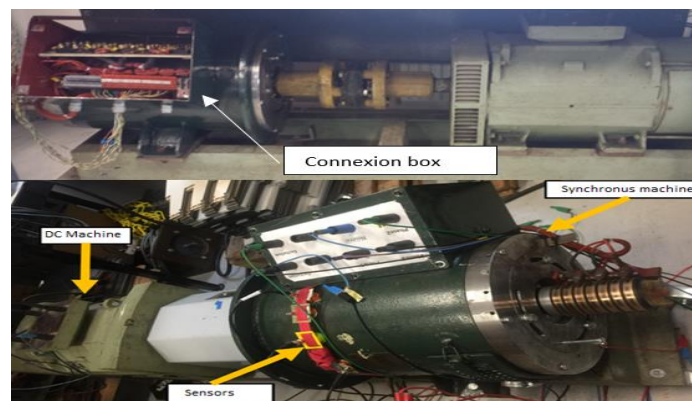


Figure 14. Experimental test bench with special synchronous generator modified to enable inter-turn short circuits.

For diagnosis, we use data obtained from the signals delivered by two flux sensors which are 180° spatially shifted around the frame of the machine as shown in Figure 8b. Here, the load induces a variation of the spectral line delivered by both sensors at 750 Hz. For presented results, a single turn is short-circuited (0.26%) in phase A of the stator. Figure 15a gives the variations of the line in healthy conditions and Figure 15b, in faulty ones. Figure 15c,d shows the zoom of harmonics variation in the faulty case for signals measured in Pos. 1 and Pos. 2. One can notice in a healthy case an identical evolution of the spectral line with load variation. In the faulty case, it is measured an increase in position 2 and a wave variation in position 1. This asymmetry evolution is in agreement with (22), (23), and phasor diagram presented in Figure 7. For the experimental tests, the synchronous machine has been modified, permitting a small short-circuit fault.

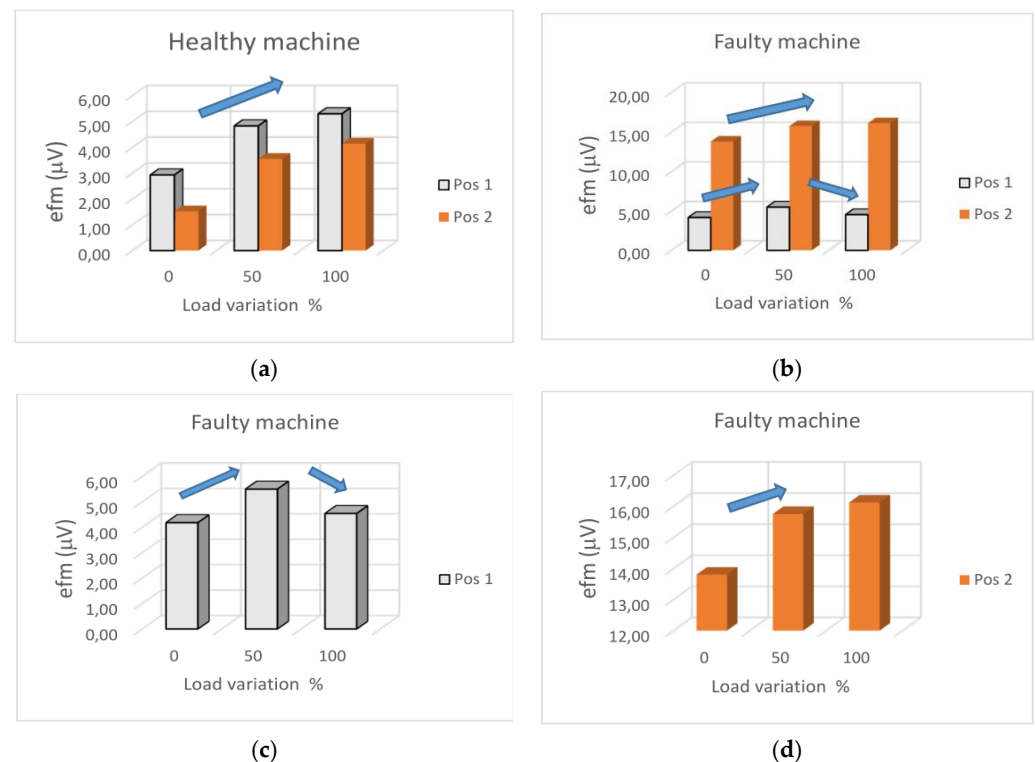


Figure 15. Harmonic components at 750 Hz under both measurement positions for synchronous generator operating at variable load: (a) healthy case, (b) faulty case, (c) faulty case in position 1, (d) faulty case in position 2.

4.5. Self-Excited Induction Generator

To confirm the applicability of the proposed method, another test has been carried out with an induction machine operating as a self-excited induction generator in a balanced and unbalanced load as it is indicated in Figure 16. This machine is a three-phase squirrel cage induction generator with 4 poles, 50 Hz, 3 kW, 380/660 V, 7.3/4.2 A, 1420 rpm, 54 stator slots, and 36 rotor bars ($N_s = 27$, $N_r = 18$).

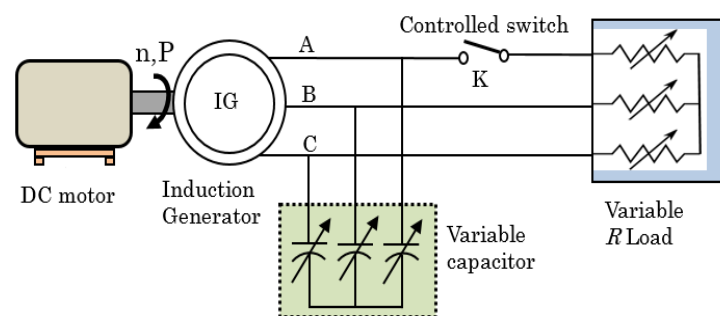


Figure 16. Self-excited induction generator connected to a resistive balanced and unbalanced load.

This machine does not offer the possibility to create artificial faults, but tests with variable frequency and the unbalanced load was carried out in order to estimate the reliability of the method in case of an unbalanced load. Actually, the aim is to check that the method provides a healthy response in unbalanced operating conditions. For IM operating as SEIG, the frequency changes with load and reactive power. If an unbalanced load appears, the symmetry of the magnetic field around the machine will be disturbed. However, this dissymmetry should not be confused with that created by a stator short-circuit fault.

For the tests, a resistive load star connected is used and the unbalanced case is obtained by disconnecting phase A of the SEIG from the load. The reactive power is kept constant and the flux sensors are placed 180° spatially shifted around the machine frame.

In this case, the frequency changes with the slip which is negative in generator operating condition ($s < 0$). Figure 17a shows the harmonic evolution for the load variation in balanced mode. Here, the line at 564 Hz (corresponding to $s = -3.5\%$, $k_r = -1$ and fundamental harmonic frequency 32 Hz) evolves in the same direction when the load increases.

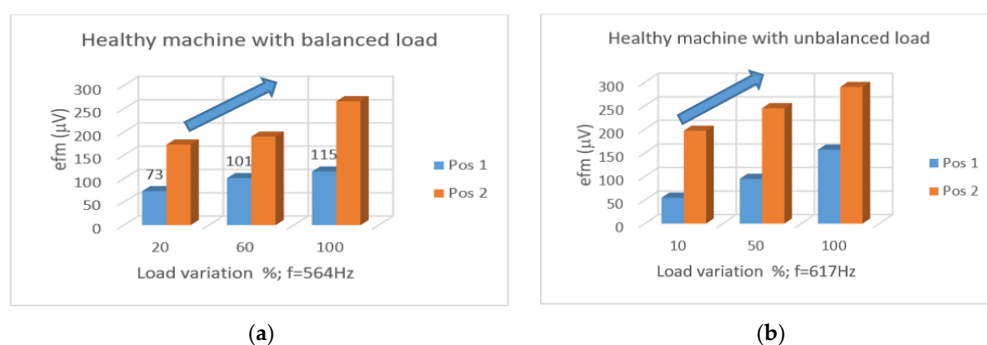


Figure 17. Amplitude variation for SEIG harmonic components at load variation: (a) healthy machine with balanced resistive load, (b) healthy machine with unbalanced resistive load.

In practice, the studied line moves with the slip, but here it will be identified as the line at 564 Hz. The time variation of the electromotive force measured by both sensors and the spectrum of the signal delivered by sensor 1 in a balanced case are presented in Figure 18. We can notice identical emf curves measured by flux sensors in Pos. 1 and Pos. 2. As in 11 kW IM, the analyzed harmonics is chosen to take into account (10) and the highest measured value.

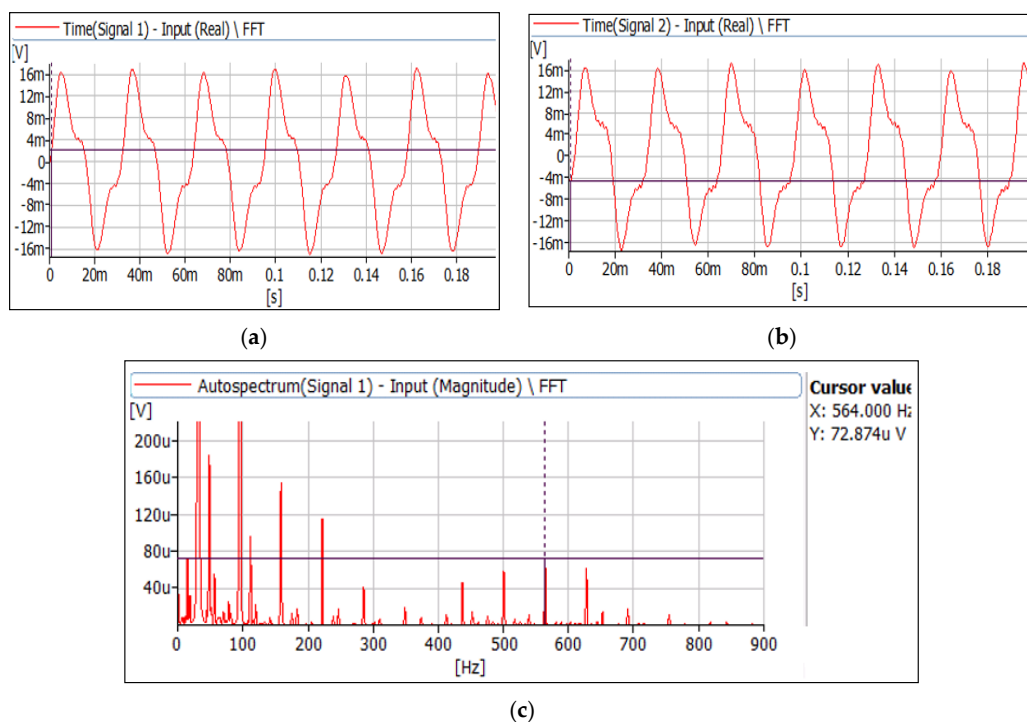


Figure 18. Signals measured by the flux sensors for balanced load: (a) emf measured in position 1, (b) emf measured in position 2, (c) signal spectrum delivered from flux sensor in position 1.

Figure 17b shows the magnitude of the line at 617 Hz (36 Hz for the fundamental harmonic frequency) in the case of unbalanced resistive load connected at the SEIG output.

In this case (which is not a faulty case), the lines show the same variation in the two measurement positions although the emf curves shown in Figure 19 are not identical.

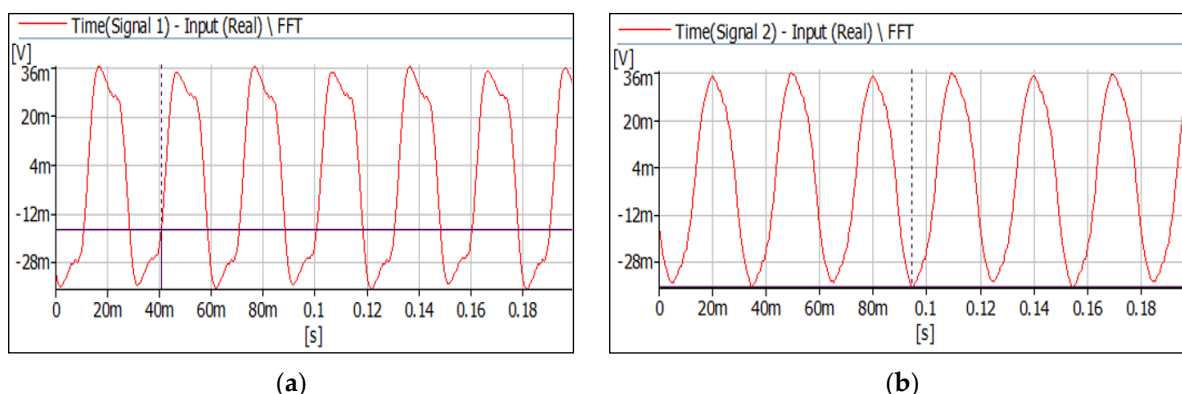


Figure 19. Signals measured by the flux sensors for unbalanced load: (a) emf measured in position 1, (b) emf measured in position 2.

This test confirms that the proposed method is sensitive to field disturbance generated by the short-circuit current and is not sensitive to frequency variation or unbalanced load.

4.6. Practical Precautions

The method is applicable for the diagnosis of all AC machines (motors and generators) uses in an industrial process, except 2 pole machines because it does not generate a dissymmetry in the phase winding. It uses the stray external magnetic field which is an image of the air-gap flux density attenuated by the stator magnetic circuit. By measuring the field, a difference can be observed which appears between the specific amplitudes (850 Hz, 750 Hz) of the magnetic spectrum in two specific positions around the machine. As the difference appears in the faulty machine but also in the healthy case, the load (which generally is a disturbing factor) is used here for discrimination. The method consists in comparing the signals delivered by each sensor during of the load variation. As shown in Figure 12a, the sensitive harmonic increases in the healthy case for Pos. 1 and Pos. 2 when the load increases. Whereas, in the faulty case, the increase of the load leads to a decrease followed by an increase (Figure 12c). This asymmetric amplitude variation between Pos. 1 and Pos. 2 is used for diagnosis and it does not require a high level of expertise to analyze the data. It concerns:

- the kind of sensor: the sensor has to be small enough so that one can consider that the measured value of the flux density is the same as the flux density at the center of the sensor. In order to get an acceptable value of the output voltage, the small size has to be compensated by the number of turns. But as the increase of the number of turns decreases the resonance frequency of the sensor, this latter has to be checked with an impedance analyzer to get sure that the frequency resonance is far from the analyzed frequency. The used sensors are 3.2 cm diameter and 1200 turns, which leads to a resonance frequency at 93 KHz.
- the location of the sensors: both sensors have to be placed symmetrically from the machine axis, approximately in the middle of the stator, between the end bells. Concerning the accuracy of the symmetry of the sensors, it increases when the pole pair number p of the machine is high. Actually, an error in the sensor alignment will be multiplied by p and it could not be possible to consider that the first terms of (22) and (23) are the same, leading to a disturbance in the diagnosis method.
- the number of measurements: practical tests have shown that when the sensors are far from the axis of the damaged coil, the results give the impression that the machine is healthy because the magnitudes at sensitive spectral lines always vary in the same direction with the load variation. Theoretically, this can be taken into

account considering all the elementary components of Tables 2 and 4 instead of the predominant components grey highlighted. To avoid this confusion, it is necessary to perform several measurements such as at least one is closer to the faulty winding than the healthy winding, among the p windings that constitute a whole phase. Consequently, the minimal number of measurements should be $2p$, but to increase the probability of fault detection, we recommend $3p$ measurement. Of course, in a practical point of view, the locations of the sensors have to take into account the non-accessible areas, e.g., the areas of the mounting base or the terminal box (Figure 20).

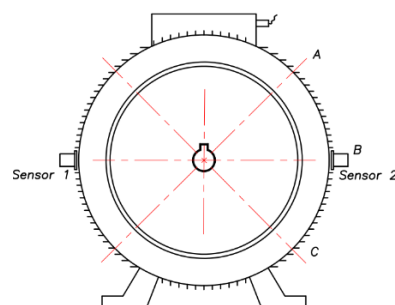


Figure 20. Illustration of the 3 measured positions of the sensors around the machine.

Then, when the obtained results give at least one position with opposed magnitude variations with the load, then a fault can be suspected. AI methods can be also used to limit the number of measurements [36].

- case of inverter fed: it should be checked that the chopping frequency is higher than the sensitive one.

5. Conclusions

This paper presents the application and the reliability of a noninvasive procedure for the detection of inter-turn short-circuit faults in the stator winding of induction and synchronous machines. This procedure uses the stray external magnetic field measured in the vicinity of the AC machines by two sensors placed at a specific angular shift to extract information about the faulty state of the machines. The analysis is carried out considering the change of the transverse field obtained from the air-gap flux density which brings up the properties related to the characteristics of the flux density components being found in the transverse external field. The new contribution of the proposed diagnosis method is the analysis strategy which eliminates the main disadvantage presented by other diagnosis methods using the comparison with a healthy state assumed to be known before the fault appears. Moreover, the described procedure is non-invasive and inexpensive, characterized by the exploitation of the spatial dissymmetry of the field created by a short circuit current in the area where the fault appears. This dissymmetry modifies the rotor slotting harmonics and induces specific signatures in the external magnetic field spectrum which are analytically demonstrated, identified, and presented in this paper. In order to eliminate the constructive dissymmetry which exists practically, the presented diagnosis method proposes a procedure where the external field is measured in the vicinity of the electrical machine in the two cases: loaded and not-loaded machine. In order to test the reliability of the method, different I_{sc} levels and an unbalanced load are tested. The paper shows that the proposed procedure can be applied to induction and synchronous machines with wound smooth rotor, considering specific spectral lines for each machine, with frequencies depending on the number of rotor slots. These specific frequencies facilitate the use of this procedure in the presence of other magnetic fields as is the case in an industrial environment. It is also shown that unbalanced operating conditions does disturb the procedure, especially in the healthy case.

Author Contributions: Data curation, E.T., I.N.; Formal analysis, R.P., R.R. and A.C.; Funding acquisition, P.L. All authors have read and agreed to the published version of the manuscript.

Funding: University Agency of Francophonie” (UAF), the Institute of Atomic Physics Bucharest and LSEE.

Institutional Review Board Statement: Not applicable.

Informed Consent Statement: Not applicable.

Acknowledgments: The authors would like to thanks the “Francophone University Agency” (FUA) (Agence Universitaire de la Francophonie) and the Institute of Atomic Physics Bucharest for the financial support brought by Contract No. 19-AUF.

Conflicts of Interest: The author declared no potential conflicts of interest with respect to the research, authorship, and/or publication of this article.

Abbreviations

p	number of pole pair
f	supply frequency
n^s	number of turns in series for a whole phase
n'^s	number of turns in an elementary section
y	number of shorted turns
N^s, N^r	number of stator and rotor slots per pole pair
I_0^s	rms value of the no load stator current
I_{sc}^s	rms value of the short circuit current
ε	air gap resultant m.m.f—healthy machine
λ	air gap permeance
b	air gap flux density- healthy machine
b^x	external radial flux density—healthy machine
h, h^s	m.m.f rank
k_s, k_r	permeance rank
$b_{h^s k_s k_r}$	elementary component of air-gap flux density
b_{KH}	component of air gap flux density
K	frequency rank of a flux density component
H	pole pair number of a flux density component
b_K^x	rank K harmonic of b^x
C_H	attenuation coefficient
R_{int}^s, R_{ext}^s	inner and outer radius of the stator
All the parameters and variables with “sc” lower index are related to the short circuit turns.	

References

1. Sadeghi, I.; Ehya, H.; Faiz, J.; Akmal, A.A.S. Online condition monitoring of large synchronous generator under short circuit fault—A review. In Proceedings of the IEEE International Conference on Industrial Technology (ICIT), Lyon, France, 19–22 February 2018; pp. 1843–1848.
2. Ondel, O.; Boutleux, B.E.; Clerc, G. Coupling Pattern Recognition with State Estimation Using Kalman Filter for Fault Diagnosis. *IEEE Trans. Ind. Electron.* **2012**, *59*, 4293–4300. [\[CrossRef\]](#)
3. Skowron, M.; Wolkiewicz, M.; Orłowska-Kowalska, T.; Kowalski, C.T. Effectiveness of selected neutral network structures based on axial flux analysis in stator and rotor winding incipient fault detection of inverter-fed induction motors. *Energies* **2019**, *12*, 2392. [\[CrossRef\]](#)
4. Bachir, S.; Tnani, S.; Trigeassou, J.C.; Champenois, G. Diagnosis by parameter estimation of stator and rotor faults occurring in induction machines. *IEEE Trans. Ind. Electron.* **2006**, *53*, 963–973. [\[CrossRef\]](#)
5. Tsypkin, M. Induction motor condition monitoring: Vibration analysis technique—Diagnosis of electromagnetic anomalies. *IEEE Autotestcon.* **2017**, 1–7. [\[CrossRef\]](#)
6. Artigao, E.; Honrubia-Escribano, A.; Gomez-Lazaro, E. In service wind turbine DFIG diagnosis using current signature analysis. *IEEE Trans. Ind. Electron.* **2020**, *67*, 2262–2271. [\[CrossRef\]](#)
7. Thomson, W.T.; Fenger, M. Current signature analysis to detect induction motor faults. *IEEE Ind. Appl. Mag.* **2001**, *7*, 26–34. [\[CrossRef\]](#)

8. Benbouzid, M.E.H. A review of induction motors signature analysis as a medium for faults detection. *IEEE Trans. Ind. Electron.* **2000**, *47*, 984–993. [[CrossRef](#)]
9. Henao, H.; Razik, H.; Capolino, G.A. Analytical approach of the stator current frequency harmonics computation for detection of induction machine rotor faults. *IEEE Trans. Ind. Appl.* **2005**, *41*, 801–807. [[CrossRef](#)]
10. Khezzar, A.; Kaikaa, M.Y.; Oumaamar, M.E.K.; Boucherma, M.; Razik, H. On the use of slot harmonics as a potential indicator of rotor bar breakage in the induction machine. *IEEE Trans. Ind. Electron.* **2009**, *56*, 4592–4605. [[CrossRef](#)]
11. Bossio, G.R.; De Angelo, C.H.; Bossio, J.M.; Pezzani, C.M.; Garcia, G.O. Separating broken rotor bars and load oscillations on IM Fault Diagnosis Through the Instantaneous Active and Reactive Currents. *IEEE Trans. Ind. Electron.* **2009**, *56*, 4571–4580. [[CrossRef](#)]
12. Athulya, K. Inter Turn Fault Diagnosis in Wound Rotor Induction Machine Using Wavelet Transform. In Proceedings of the 2018 International CET Conference on Control, Communication, and Computing (IC4), Thiruvananthapuram, India, 5–7 July 2018; pp. 22–27.
13. Radecki, A. Stator winding inter-turn short circuit modelling of a squirrel cage induction motor. *Power Electron. Drives* **2016**, *1*, 140–148. [[CrossRef](#)]
14. Bouzida, A.; Touhami, O.; Ibtouen, R.; Belouchrani, A.; Fadel, M.; Rezzoug, A. Fault diagnosis in industrial induction machines through discrete wavelet transform. *IEEE Trans. Ind. Electron.* **2011**, *59*, 4385–4395. [[CrossRef](#)]
15. Azzoug, Y.; Pusca, R.; Sahraoui, M.; Ammar, A.; Romary, R.; Cardoso Marques, A.J. A Single Observer for Currents Estimation in Sensor's Fault-Tolerant Control of Induction Motor Drives. In Proceedings of the ICAAID2019, International Conference on Applied Automation and Industrial Diagnostics, Elazig, Turkey, 25–27 September 2019; pp. 1–6.
16. Panagiotou, P.A.; Arvanitakis, I.; Lophitis, N.; Antonino-Daviu, J.A.; Gyftakis, K.N. Analysis of Stray Flux Spectral Components in Induction Machines under Rotor Bar Breakages at Various Locations. In Proceedings of the ICEM'18, XIII International Conference on Electrical Machines, Alexandroupoli, Greece, 3–6 September 2018; pp. 2345–2351.
17. Tavner, P.J.; Hammond, P.; Penman, J. Contribution to the study of leakage fields at the ends of rotating electrical machines. *IEE* **1978**, *125*, 1339–1349. [[CrossRef](#)]
18. Kameari, A. Three dimensional eddy current calculation using finite element method with A-V in conductor and in vacuum. *IEEE Trans. Magn.* **1988**, *24*, 118–121. [[CrossRef](#)]
19. Ceban, A.; Fireteanu, V.; Romary, R.; Pusca, R.; Taras, P. Finite Element Diagnosis of Rotor Faults in Induction Motors based on Low Frequency Harmonics of the Near-Magnetic Field. In Proceedings of the SDEMPED 2011, IEEE International Symposium on Diagnostics for Electric Machines, Power Electronics and Drives, Bologna, Italy, 5–8 September 2011; pp. 192–198.
20. Canova, A.; Manzin, A.; Tartaglia, M. Evaluation of different analytical and semi-analytical methods for the design of ELF magnetic field shields. *IEEE Trans. Ind. Appl.* **2002**, *38*, 788–796. [[CrossRef](#)]
21. Romary, R.; Roger, D.; Brudny, J.F. Analytical computation of an AC machine external magnetic field. *Eur. Phys. J. Appl. Phys.* **2009**, *47*, 31102. [[CrossRef](#)]
22. Frosini, L.; Borin, A.; Girometta, L.; Venchi, G. A novel approach to detect short circuits in low voltage induction motor by stray flux measurement. In Proceedings of the ICEM'12, 20th International Conference on Electrical Machines, Marseille, France, 2–5 September 2012; pp. 1536–1542.
23. Henao, H.; Demian, C.; Capolino, G.A. A frequency-domain detection of stator winding faults in induction machines using an external flux sensor. *IEEE Trans. Ind. Appl.* **2003**, *39*, 1272–1279. [[CrossRef](#)]
24. Romary, R.; Corton, R.; Thailly, D.; Brudny, J.F. Induction machine fault diagnosis using an external radial flux sensor. *Eur. Phys. J. Appl. Phys.* **2005**, *32*, 125–132. [[CrossRef](#)]
25. Vitek, O.; Jada, M.; Hajek, V.; Bauer, P. Detection of eccentricity and bearing faults using stray flux monitoring. In Proceedings of the SDEMPED 2011, IEEE International Symposium on Diagnostics for Electric Machines, Power Electronics and Drives, Bologna, Italy, 5–8 September 2011; pp. 456–461.
26. Ceban, A.; Pusca, R.; Romary, R. Study of rotor faults in induction motors using external magnetic field analysis. *IEEE Trans. Ind. Electron.* **2012**, *59*, 2082–2093. [[CrossRef](#)]
27. Cabanas, M.F.; Melero, M.G.; Orcajo, G.A.; Rodriguez, F.F.; Sariego, J.S. Experimental application of axial leakage flux to the detection of rotor asymmetries, mechanical anomalies and interturn short circuits in working induction motors. In Proceedings of the ICEM98, International Conference on Electrical Machines, Istanbul, Turkey, 2–4 September 1998; pp. 420–425.
28. Assaf, T.; Henao, H.; Capolino, G.A. Simplified axial flux spectrum method to detect incipient stator inter-turn short-circuits in induction machine. In Proceedings of the ISIE 2004, IEEE International Symposium on Industrial Electronics, Ajaccio, France, 4–7 May 2004; pp. 815–819.
29. Kia, S.H.; Henao, H.; Capolino, G.A.; Martis, C. Induction machine broken bars faults detection using stray flux after supply disconnection. In Proceedings of the IECON 2006, 32th Annual Conference of the IEEE Industrial Electronics Society, Paris, France, 7–10 November 2006; pp. 1498–1503.
30. Schmerber, L.; Rouve, L.L.; Foggia, A. Original 2D cylindrical harmonics method of the near magnetic stray field of an electrical motor. In Proceedings of the IEMDC 2005, IEEE International Electric Machines and Drives Conference, San Antonio, TX, USA, 15–18 May 2005; pp. 92–98.
31. Penman, J.; Sedding, H.G.; Fink, W.T. Detection and location of interturn short circuits in the stator windings of operating motors. *IEEE Trans. Energy Convers.* **1994**, *9*, 652–658. [[CrossRef](#)]

-
32. Pusca, R.; Romary, R.; Ceban, A.; Brudny, J.F. An online universal diagnosis procedure using two external flux sensors applied to the AC electrical rotating machines. *Sensors* **2010**, *10*, 7874–7895. [[CrossRef](#)] [[PubMed](#)]
 33. Brudny, J.F. Modélisation de la denture des machines asynchrones. *Phénomène Résonance J. Phys. III* **1997**, *7*, 1009–1023. [[CrossRef](#)]
 34. Pusca, R.; Romary, R.; Ceban, A. Detection of inter-turn short circuit in induction machines without knowledge of the healthy state. In Proceedings of the ICEM '12, 20th International Conference on Electrical Machines, Marseille, France, 2–5 September 2012; pp. 1637–1642.
 35. Thailly, J.D.; Romary, R.; Roger, D.; Brudny, J.F. Attenuation of magnetic field components through an AC machine stator. *COMPEL* **2008**, *27*, 744–753. [[CrossRef](#)]
 36. Pusca, R.; Demian, C.; Mercier, D.; Lefevre, E.; Romary, R. Improvement of a diagnosis procedure for AC machines using two external flux sensors based on a fusion process with belief functions. In Proceedings of the IECON 2012, 38th Annual Conference of the IEEE Industrial Electronics Society, Montreal, QC, Canada, 25–28 October 2012; pp. 5078–5083.